AIChE

Photon Absorption in a Hybrid Slurry Photocatalytic Reactor: Assessment of Differential Approximations

Sayra L. Orozco, Heidi I. Villafán-Vidales, and Camilo A. Arancibia-Bulnes
Departamento de Sistemas Energéticos, Centro de Investigación en Energía,
Universidad Nacional Autónoma de México, Temixco, Morelos 62580, México

DOI 10.1002/aic.13712
Published online December 7, 2011 in Wiley Online Library (wileyonlinelibrary.com).

Radiative transfer inside a slurry photocatalytic reactor with hybrid illumination from both solar radiation and lamps is examined. The local volumetric rate of photon absorption is evaluated. For this purpose, the P1 and the modified differential approximations (MDAs) are used, and results compared to a solution by the Monte Carlo method. It is found that significant differences may arise between the predictions of the above approximations and the exact results provided by the Monte Carlo simulations. The P1 approximation is very inaccurate near to the radiation entrance for the partially collimated solar radiation, although it improves, as optical depth increases. As expected, the MDA improves the results near to the boundary. Surprisingly, it turns out to be much worse than the P1 approximation at medium and large optical depths. In the case of lamp irradiation, the behavior of the MDA is the opposite; it works better at small optical depths. © 2011 American Institute of Chemical Engineers *AIChE J,* 58: 3256–3265, 2012
Keywords: photocatalytic reactor, solar energy, radiation transport, Monte Carlo method, modified differential approximation

Introduction

Heterogeneous photocatalysis is an attractive wastewater treatment method for the elimination of organic pollutant,[1,2] which becomes an environment friendly technique, when solar energy is used as a light source for the process.[3,4] Either if solar or artificial sources are considered, radiative transfer is a central part in the modeling of photocatalytic reactions.[5] There are many instances of the design of these reactors where radiative processes must be taken into account; for instance, if one is interested in comparing reactors with different geometries and light sources. Also, for the scaling up of processes, this kind of modeling is necessary. The reason is that the apparent kinetics of a reaction may be affected by many factors, among them the optical ones: reactor geometry, type of light source, optical properties of the involved surfaces and windows, optical properties, and concentration of the catalyst. Thus, radiative transfer modeling helps to obtain kinetic parameters that are independent of that factors.[6–8]

In particular, in slurry photocatalytic reactors, scattering of radiation by submicrometer catalyst particles plays an important role[9]; not only catalyst particles absorb light but also they produce very strong scattering effects, due to the high refractive index of the material. Modeling radiative transfer processes in such scattering media is considerably more complicated than in purely absorbing environments. If one is interested in evaluating the energy absorbed at each volume element inside the reactor (the so-called local volumetric rate of photon absorption, LVRPA), in principle one must solve the radiative transfer equation (RTE).[10–12]

Analytical solutions to the RTE are only possible in a few simplistic (and unrealistic) cases. Different authors have addressed the solution of the RTE in more realistic situations by a variety of methods (see Refs. 2 and 5 and references therein). For instance, it is possible to solve complex radiative transfer problems exactly, using numerical methods.[8,13–15] As those methods can be cumbersome, considerable attention has been paid also to approximate analytical solutions.[7,16–18] For instance, many-flux models are attractive due to their ease of implementation.[6,17,19,20]

One very popular method is the P1 approximation.[10] It is also known as the differential approximation, because it transforms the complicated integro-differential RTE into a more manageable partial differential equation. This approximation has been applied to several photocatalytic reactors,[7,21–24] like parabolic trough and tubular solar photoreactors, as well as an annular lamp photoreactor. However, as it happens with many of the approximate methods, the P1 approximation has been tested against exact numerical solutions of the RTE only in a few restricted situations.

In this work, we address the comparison of the P1 approximation against the Monte Carlo (MC) numerical method. In particular, we use a hybrid photocatalytic reactor (HPR), which operates with both lamps and sunlight,[7] as a test model. In this comparison, we also include a variation of the P1 approximation, known as modified differential approximation (MDA).[10,11,25,26] This approximation was devised[26] to overcome one of the main limitations of the former; namely, the assumption of nearly diffuse radiative intensity at every point inside the participating medium (reaction space), a condition not always fulfilled in practice.

Correspondence concerning this article should be addressed to S. L. Orozco at caab@cie.unam.mx.
C. A. Arancibia-Bulnes: On sabbatical leave at Departamento de Ingeniería Química y Metalurgia, Universidad de Sonora.

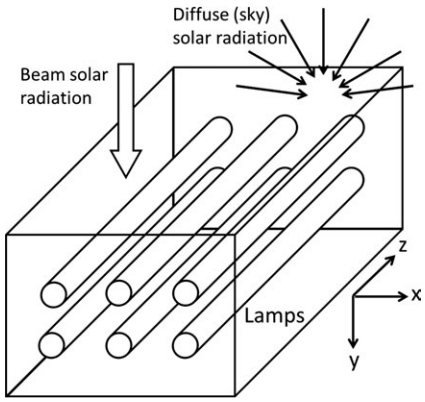

Figure 1. Physical model of the problem.

As will be discussed below, significant differences are found between the P1 and the MC solutions for the problem at hand. Moreover, contrary to expectations, it is also found that the MDA is not necessarily an improvement over the P1 method.

Physical Model

The HPR was devised to allow for a continuous operation of the photocatalytic process even in the absence of sunlight,[7] or in low irradiance conditions, using lamps as backup light source. Also, it allows providing a higher level of illumination to the interior of the reaction space, when dealing with opaque solutions. It consists of an acrylic rectangular box, as illustrated in Figure 1, with dimensions $0.50 \times 0.30 \times 0.66$ m^3. Solar radiation enters through the upper face of the reactor, and artificial light is provided by six cylindrical lamps (either UV or visible). Lamps are inserted through the smaller lateral faces, inside 4.4-cm diameter glass tubes that run across the box. They are distributed in the reactor in such a way that each of them illuminates equivalent volumes; that is, the reactor is divided into six equal rectangular volume elements, and a lamp is located at the center of each of them. The reactor walls are reflective. More details are given in Ref. 7.

Theoretical Methods

The most relevant radiative quantity to evaluate in photocatalytic reactors is the LVRPA. This quantity gives the number of photons moles (also called einstein, E) absorbed by the catalyst at point **r**, per unit suspension volume. Mathematically, the LVRPA is given by

$$e_{\mathrm{L}}(\mathbf{r}) = \int_0^\infty L_\lambda(\mathbf{r}) d\lambda \tag{1}$$

where the quantity integrated with respect to wavelength is the spectral LVRPA

$$L_\lambda(\mathbf{r}) = \frac{1}{hcN_{\mathrm{A}}} \lambda \kappa_\lambda G_\lambda(\mathbf{r}) \tag{2}$$

Here, the local incident radiation G_λ (**r**) is used, which is the sum of radiation contributions arriving at a given point **r** from all possible directions and is the quantity addressed by the analytical models to be discussed here.

In the discussion to follow and for the sake of simplicity, the subscript λ will be omitted from all quantities. Nevertheless, it is implicit that all radiative variables and parameters are spectrally dependent.

The P1 approximation

The P1 approximation is an analytical approximation to the RTE, based on the assumption that at any point inside the reactor volume, the radiation field arrives from all directions with nearly equal intensity.[10] This assumption transforms the integro-differential RTE into a second-order partial differential equation, so it is also known as the differential approximation.

$$\nabla^2 G(\mathbf{r}) = k_{\mathrm{d}}^2 G(\mathbf{r}) \tag{3}$$

where the transport constant k_{d} is called radiation diffusion coefficient.

$$k_{\mathrm{d}} = \sqrt{3\kappa\beta(1-\omega g)} \tag{4}$$

Here β is the extinction coefficient of the medium, which is the sum of the scattering σ and absorption κ coefficients. These coefficients are proportional to the concentration of catalyst particles C_{cat}. The proportionality constants are known as specific extinction, absorption, and scattering coefficients, and they have been measured for several commercial TiO_2 brands.[9,27] The ratio between the scattering and the extinction coefficients is called the scattering albedo $\omega = \sigma/\beta$.

The MDA

The assumption of almost perfectly isotropic propagation of radiation inside the reactor may not be true in many cases. In particular, it is expected to give the worst results near to transparent boundaries through which radiation is entering, especially if radiation entering the reactor is highly directional.[25] This is the case with the beam component of solar radiation. In particular, in the UV portion of the solar spectrum, beam radiation is present in similar amounts to diffuse radiation (see for instance the solar spectra reported by Hulstrom et al.[28]). Because of this, incidence of a non-negligible directional component of radiation occurs on the surface of directly illuminated solar reactors, which points out to a potential failure of the P1 approximation.

To improve the accuracy of the method in situations where collimated light plays an important role, the MDA[26] was developed, as a modification of the P1 approximation. This approximation treats differently the collimated and the diffuse components. The intensity of radiation at any point is regarded as the sum of these two components. The collimated component is not difficult to analyze, because it is attenuated according to the Lambert–Beer's law, due to both absorption and scattering. Radiation scattered from the collimated beam automatically becomes diffuse. Therefore, the equation for the diffuse component differs from the standard P1 approximation by the addition of a source term, accounting for the contribution from scattered collimated radiation. The local incident radiation may be expressed as a sum

$$G(\mathbf{r}) = G_{\mathrm{c}}(\mathbf{r}) + G_{\mathrm{d}}(\mathbf{r}) \tag{5}$$

The collimated component G_{c} (**r**) is given in terms of the intensity of collimated incident beams

$$G_{\mathrm{c}}(\mathbf{r}) = \int_{4\pi} I_{\mathrm{c}}(\mathbf{r}, \hat{\mathbf{s}}_{\mathrm{c}}) d\Omega \tag{6}$$

In the case of a single beam of radiation impinging with direction $\hat{\mathbf{s}}_{\mathrm{c}}$, and for an interface reflectance of ρ_{c} ($\hat{\mathbf{s}}_{\mathrm{c}}$) the collimated contribution becomes

$$G_c(\mathbf{r}) = \left[1 - \rho_c(\hat{\mathbf{s}}_c)\right] q_{c,0} \int_{4\pi} \delta(\hat{\mathbf{s}} - \hat{\mathbf{s}}_c[(\mathbf{r})]) \exp(-\tau_c) d\Omega \quad (7)$$

The differential equation for the diffuse component is similar to the P1 approximation, with the addition of a nonhomogeneous term

$$\nabla^2 G_d(\mathbf{r}) - k_d^2 G_d(\mathbf{r}) = -3 q_c \beta \sigma (1 - \rho_c)[g + (1 - \omega g)] \quad (8)$$

where

$$q_c = q_{c,0} \exp(-\beta y / \cos\theta_c) \quad (9)$$

where is θ_c the incidence; that is, the angle between $\hat{\mathbf{s}}_c$ and the surface normal.

Boundary conditions

To solve for the incident radiation, it is necessary to have boundary conditions which can be used together with Eq. 3 or 8. Marshak boundary condition,[10,29] modified for semi-transparent boundaries,[30] is considered

$$(1 - 2\rho_1) G_d(\mathbf{r}) - 2(1 + 3\rho_2)[3\beta(1 - \omega g)]^{-1} \hat{\mathbf{n}} \cdot \nabla G_d(\mathbf{r}) = \Gamma(\mathbf{r}) \quad (10)$$

In the case of the P1 approximation, this boundary condition applies to the whole incident radiation G ($\mathbf{r}$), and the term $\Gamma(\mathbf{r})$ in the right hand side of Eq. 10 should be made equal to zero. For the MDA, this only applies to the diffuse component G_d ($\mathbf{r}$), while $\Gamma(\mathbf{r})$ is given by

$$\Gamma(\mathbf{r}) = 4 q_{d,0} - [2\omega g(1 + 3\rho_2)](1 - \omega g)^{-1}(1 - \rho_E) \cos\theta_c q_{c,0} \quad (11)$$

In Eq. 10, $\check{\mathbf{n}}$ stands for the unit vector normal to the boundary, and ρ_i is the ith moment of the surface reflectance function, defined as

$$\rho_i = \int_0^{\frac{\pi}{2}} \rho(\cos\theta) \cos^i\theta \sin\theta \, d\theta \quad (12)$$

The radiative flux $q_{d,0}$ is the diffuse component of the incident solar irradiance, given by a standard AM1.5 solar spectrum over the UV range,[28] and τ_1 is the first moment of the surface transmittance function.

$$\tau_1 = \int_0^{\frac{\pi}{2}} \tau(\cos\theta) \cos\theta \, d\theta \quad (13)$$

The parameters ρ_i and τ_1 were determined considering the optical properties of the HPR.

Analytical solutions to the models

To solve Eq. 8, the solar and the artificial components of the radiation field were analyzed separately. For the solar diffuse component, Eq. 8 was written in a rectangular coordinate system, as solar irradiance is uniform over the top of the reactor and can be neglected on the walls. Also, the radiative properties of the glass sheet show a directional dependence with the polar angle only. Therefore, considering azimuth symmetry, the diffuse radiation G_d varies only in the vertical direction (y axis)

$$\frac{d^2 G_d}{dy^2} - k_d^2 G_d = -3 q_c \beta \sigma (1 - \rho_c)[g + (1 - \omega g)] \quad (14)$$

Equation 14 is a second-order nonhomogeneous ordinary differential equation and its solution is given by

$$G_d(y) = A \exp(-\beta y / \cos\theta_c) + C_1 \exp(-k_d y) + C_2 \exp(k_d y) \quad (15)$$

The last two terms of the right hand side of this equation are the solution to the homogeneous equation, which corresponds to the P1 approximation. The first term accounts for the contribution of collimated solar radiation, which transforms into diffuse radiation by means of scattering.

$$A = -3\beta\sigma q_{c,0}(1 - \rho_c)[g + (1 - \omega g)]\left[\left(\beta^2 / \cos^2\theta_c\right) - k_d^2\right]^{-1} \quad (16)$$

For the collimated solar component, Eq. 7 is applied, giving

$$G_c(y) = (1 - \rho_c) q_{c,0} \exp(-\beta y / \cos\theta_c) \quad (17)$$

Substitution of the solutions (15) and (17) in the boundary condition (10) allows for obtaining the values of the coefficients C_1 and C_2 (see the Appendix).

When there is no collimated incident radiation (beam solar radiation), $q_c = 0$ the above solution reduces to that of the P1 approximation; that is, $A = E = 0$

$$G(y) = B_1 \exp(-k_d y) + B_2 \exp(k_d y) \quad (18)$$

where the coefficients B_1 and B_2 are also given in the Appendix.

For the lamps, Eq. 3 is written in cylindrical coordinates. The considerations were that the emissive power is independent of the angular variable ϕ, and the lamp is long enough, so that end effects are negligible; that is, there is no dependence with respect to the z-coordinate (along the lamps). Then, the equation for the artificial component from each lamp depends on the radial coordinate only. Moreover, lamp emission was considered diffuse, so the MDA and P1 are identical in this case

$$\frac{d^2 G}{dr^2} + \frac{1}{r}\frac{dG}{dr} - k_d^2 G = 0 \quad (19)$$

Equation 19 is a modified Bessel's equation, which has a general solution of the form

$$G(k_d r) = C_3 I_0(k_d r) + C_4 K_0(k_d r) \quad (20)$$

where I_0 and K_0 are zeroth-order modified Bessel functions of the first and second kind, respectively. The first of these functions cannot be present in the solution, because it gives an increase of G with the distance from the lamp, which is an unphysical behavior. Therefore, $C_3 = 0$ and

$$G(k_d r) = C_4 K_0(k_d r) \quad (21)$$

The coefficient C_4 is obtained by application of the boundary conditions (10) and is given in the Appendix.

Finally, the incident radiation G_λ ($\mathbf{r}$) at any given point is the sum of the solar beam and diffuse contributions, Eqs. 15 and 17, and one contributions of the form (21) for each lamp. For each of the latter, the radial coordinate is

measured from the center of the lamp; that is, $r = |\mathbf{r} - \mathbf{r}_i|$. For the evaluation of each lamp contribution, at a given point, the shadowing by other lamps was considered. In the case of the P1 approximation, Eq. 20 is used for the solar contribution instead of (15) and (17).

MC method

MC is a method of statistical simulation in which the average behavior of a system is determined. To solve radiative transfer problems with this method, the radiation energy is uniformly divided into a large number of discrete energy bundles (sometimes called photons). The history of each one of these photons is traced from their emission points to their absorption points. The optical behavior of the different system components and the laws of probability are used to determine the number of photons absorbed by a given surface or volume element.[12,15]

In this work, a MC method is applied. To carry out the simulation, two types of photons are used: (a) the solar photons are the ones entering through the upper surface of the reactor. The source of this kind of photons is the sun; and (b) the lamp photons correspond to those emitted by the lamps. The power carried by the solar and lamp photons is

$$P_s = Q_s/N_s \tag{22}$$

$$P_l = Q_l/N_l \tag{23}$$

where Q_s is the solar power input, Q_l is the lamps power input, N_s and N_l are the numbers of solar and lamp photons emitted, respectively.

To methodology of the simulations is as follows: first a fixed number of solar photons are propagated one at a time, according to the rules to be described below, until their individual histories end. This may happen when a photon is absorbed in the medium or exits the reactor. Once the history of all of the solar photons has been traced, the lamp photons are propagated following the same rules, except for the point and direction of emission.

In the case of solar photons, it is first necessary to decide if they are collimated or diffuse photons. The fraction of collimated solar radiation is given by

$$p_c = q_{c,0}/(q_{c,0} + q_{d,0}) \tag{24}$$

To decide whether a given photon is collimated or diffuse, a random number uniformly distributed between 0 and 1 is generated, and compared p_c, if it is smaller than this parameter, the photon is collimated, otherwise it is diffuse. In particular, the UV solar radiation has nearly 50% beam radiation and 50% diffuse radiation, so we have taken $p_c = 0.5$.

The next step is the determination of the entrance direction of the photon with respect to the surface normal. This is defined in terms of the azimuth ϕ and polar θ angles as

$$\hat{\mathbf{s}} = \cos\ \theta\, \hat{\mathbf{n}} + \sin\ \theta\ \cos\ \phi\, \hat{\mathbf{t}}_1 + \sin\ \theta\ \sin\ \phi\, \hat{\mathbf{t}}_2 \tag{25}$$

where $\hat{\mathbf{t}}_1, \hat{\mathbf{t}}_2$ are two unit vectors, which together with the surface normal vector $\hat{\mathbf{n}}$ form an orthogonal set.

For beam radiation the polar and azimuth angles are given by the direction of the incoming radiation; that is, by the solar position vector. On the other hand, for the diffuse component, the azimuth and polar angles are randomly generated according to[12]

$$\psi = 2\pi\, \Re_\psi \tag{26}$$

$$\theta = \sin^{-1} \sqrt{\Re_\theta} \tag{27}$$

where $\Re_\psi$ and $\Re_\theta$ are uniform random numbers.

The above expressions for the polar and azimuth angles are also valid for the photons emitted from the lamp, which are regarded as perfectly diffuse; it is only necessary to take into account in Eq. 25, the appropriate normal vector for every point at the lamp's surface.

With the azimuthal angle of incidence, a transmittance is calculated according to Fresnel equations.[10] The value of this transmittance is compared with a random number to determine whether the photon enters to the reactor or is reflected. In the latest case, the photon is lost, and its history ends. If the photon is transmitted, the entrance point in the upper surface of the reactor is randomly calculated. In fact, the probability of a given photon entering at any location on this surface is uniform; therefore, the entrance coordinates $(x,0,z)$ are given by

$$x = X\Re_x \tag{28}$$

$$z = Z\Re_z \tag{29}$$

where X and Z are the lengths of the sides of the rectangular upper surface of the reactor.

For photons emitted by the lamp, the emission point over the cylindrical surface of radius R is given in terms of two coordinates, an angle ϕ and a longitudinal coordinate z, which are given by

$$\phi = 2\pi\Re_\phi \tag{30}$$

$$z = Z\Re_z \tag{31}$$

Once the entrance (or emission) position and the direction of a photon are known, the distance it travels in the participating medium to a point of collision with a particle is given by an exponential probability distribution. This exponential decay arises from the Lambert–Beer law of extinction for incident radiation in a participating medium. Accordingly, the distance is a random number given by

$$d = -\beta^{-1} \ln \Re_d \tag{32}$$

If the path length given by Eq. 32 is larger than the distance to any of the reactor walls or the lamp walls, then the photon strikes with the nearest wall. If this wall corresponds to a lateral face reactor, then the photon is specularly reflected. When the collision is given with the upper wall, there are two options: (1) the photon is reflected back into the reactor and (2) is transmitted and exits the reactor. To know which of these two options are realized for a given photon, a random number is generated and compared with the internal reflectivity value. If the photon is reflected back, it is propagated again generating a new random distance according to Eq. 32, whereas in the case of transmission, the photon history ends. Supposing that the collision occurs with a lamp wall, and then the photon is also lost.

If, on the contrary, a collision with a particle occurs before the photon reaches any of the walls, it is necessary to decide whether this collision results on an absorption or a scattering event. This is done by comparing a uniformly distributed random number with the scattering albedo of the particles. In case of absorption, a count is recorded in the

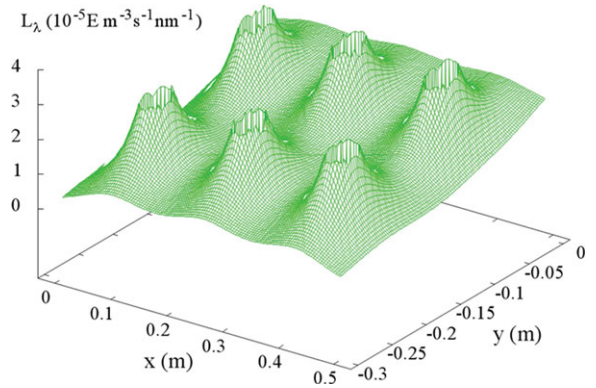

Figure 2. Spectral LVRPA in the cross section of the reactor from the MDA approximation.

[Color figure can be viewed in the online issue, which is available at wileyonlinelibrary.com.]

volume element where it occurs. On the other hand, if scattering occurs, the scattering angle θ is calculated by a random number distributed according to the scattering phase function. In particular, in this work, we have considered the Henyey–Greenstein (HG) phase function[10,15,27]

$$\Phi_{HG}(\theta) = \frac{1-g^2}{(1+g^2-2g\ \cos\ \theta)^{3/2}} \tag{33}$$

Random scattering angles can be generated according to the HG phase function by means of the following equation

$$\theta = \cos^{-1}\left\{\frac{1}{2g}\left[1+g^2-\left(\frac{1-g^2}{1+g-2g\Re_\theta}\right)^2\right]\right\} \tag{34}$$

The second angle that determines the scattered ray direction, the azimuth angle, is randomly chosen between 0 and 2π, according to Eq. 26. The scattered vector is determined by Eq. 25, where now the original propagation vector of the photon should be used instead of the surface normal.

After each scattering event, the above propagation procedure is repeated until the photon is absorbed or exits the reactor through the upper wall or collides with a lamp.

Once all photons have been emitted, the LVRPA for each volume element is obtained as

$$L = \frac{1}{hcN_A}\frac{\left(N_{i,s}P_s + N_{i,l}P_l\right)}{V_i} \tag{35}$$

where $N_{i,s}$ and $N_{i,l}$ are the numbers of solar and lamp photons absorbed at the ith volume element, respectively.

Results and Discussion

Simulations were carried out with the P1, MDA, and MC methods, to evaluate the LVRPA L_λ. For the purposes of this study, a representative wavelength of 365 nm was chosen, where Degussa P25 TiO_2 has extinction coefficient of 5.61×10^4 cm^2 g^{-1}, scattering albedo of 0.8422, and asymmetry parameter of 0.5026, as reported by Satuf et al.[27] It is important to point out that these values of the optical coefficients are for sonicated suspensions. Typically, when experiments are carried out with mechanically mixed (not sonicated), the coefficients are much smaller,[18,23,31] because the state of aggregation of the TiO_2 particles is determinant in their optical properties. Nevertheless, the results obtained here are expressed in terms of optical depth and optical thickness, to make them less dependent on the particular values of the optical coefficients used, as well as on catalyst concentration. The definition of optical depth and the optical thickness and their difference are explained as follows.

As expressed for instance by Eq. 17, a beam of radiation propagating inside an optically participative medium decays exponentially with the dimensionless variable $\tau_y = \beta y$, not with the geometrical depth y. To express this fact, the former is called optical depth. Although the decay of diffuse fluxes obeys more complicated laws, this quantity is still directly related to the degree of attenuation of radiation after traversing a given distance in the medium. The maximum value of the optical depth, the product of the extinction coefficient by the height of the reactor, is called the optical thickness of the system $\tau_H = \beta H$. In a similar manner, a radial optical depth can be defined $\tau_r = \beta r$, based on the radial distance from a lamp r. Actually, optical depths and thicknesses can be defined for every other geometrical coordinate, but they will not be used here. Finally, note that the catalyst concentration is implicitly incorporated into the optical depth, as the extinction coefficient is proportional to this concentration.

In most of the calculations, titanium dioxide concentration of 5.941 mg L^{-1} was considered, although some results are presented also for other values of this parameter. The spectral photon emission rates considered for the sources at this wavelength are $P_l = 2.25 \times 10^{-7}$ Es^{-1} nm^{-1}, for each lamp, and $P_s = 4.93 \times 10^{-7}$ Es^{-1} nm^{-1}, for solar radiation. In some cases, integration over wavelength and volume was carried out to evaluate the volumetric rate of photon absorption (VRPA) of the whole reactor. In those cases, the complete set of spectral values was taken into account for catalyst optical properties[27] and solar[28] and lamp[7] spectra.

In Figure 2, we present a graph of the distribution of the LVRPA across the reactor for combined solar and lamp illumination, as calculated from the MDA approximation. The six craters correspond to the higher illumination obtained at the walls of the lamps. Global (beam plus diffuse) solar radiation is entering at the $y = 0$ plane, which corresponds to the top face of the reactor. Beam solar radiation enters vertically. Note that, because we have assumed that the radiation

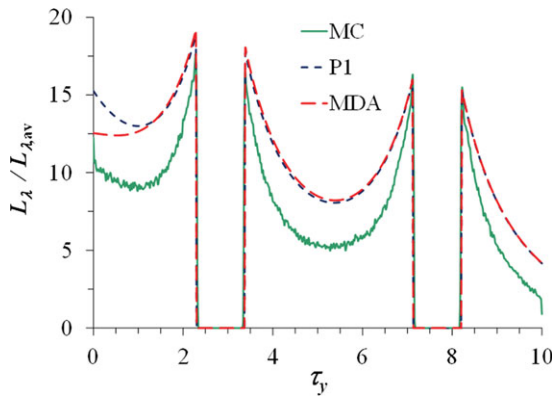

Figure 3. Normalized spectral LVRPA as a function of optical depth coordinate for illumination by both lamps and global (diffuse plus beam) solar radiation.

Comparison between different models. [Color figure can be viewed in the online issue, which is available at wileyonlinelibrary.com.]

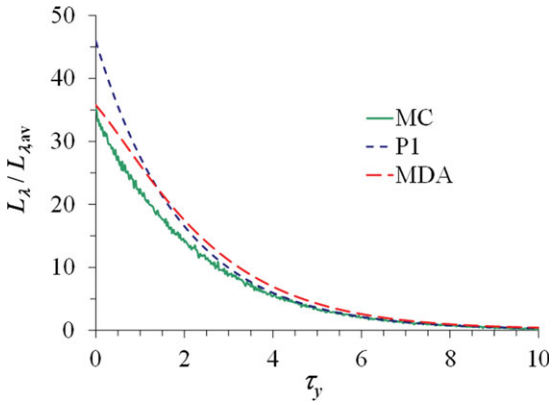

Figure 4. Normalized LVRPA as a function of optical depth coordinate for illumination by both beam and diffuse solar radiation.

Comparison between different models. [Color figure can be viewed in the online issue, which is available at wileyonlinelibrary.com.]

distribution is not dependent on the z coordinate, this distribution holds for any cross section of the reactor perpendicular to the lamps; that is, all xy planes, for any value of z. Actually, this should hold well except for short distances to the wall, equivalent to an optical depth value of one. In the present case, this corresponds to around 0.03-m distance from each wall along the lamp direction (to be compared to the 0.66-m length of the reactor).

Surfaces similar to Figure 2 can be generated also with the P1 approximation and MC method, but a visual comparison of such kind of graphs is not very instructive. We will carry out one-dimensional comparisons instead, along a vertical line that crosses the centers of two lamps; that is, a fixed value of $x = 0.33$ m. Such a comparison is presented in Figure 3.

The quantity displayed in Figure 3 and all subsequent graphs is the normalized LVRPA; that is, divided by the quantity $L_{\lambda,av}$. The latter value is a sort of "average" for the LVRPA, obtained by summing the photon emission rates from all the sources present in every case and dividing it by the volume of the reactor.

As can be observed in Figure 3, substantial differences exist between the MDA calculation and the MC method, particularly in regions far from the sources. Moreover, there are also differences between the MDA and P1, mainly at the left side of the graph (corresponding to the top of the reactor). To understand the origin of these differences, detailed comparisons are carried out below, considering the radiation sources independently of each other.

As a first comparison, we consider the case of the reactor without lamps; that is, only the suspension illuminated by solar radiation in a rectangular reaction space. Results are presented in Figure 4. It can be appreciated on this graph that the value of the LVRPA predicted by the P1 approximation near to the entrance boundary of the reactor is much larger than the exact value obtained from the MC simulations. In contrast, the MDA approximation is very accurate at this point. However, this situation is reversed at medium optical depths (between 1 and 2). Actually, there is a clear difference in the shape of the MDA approximation curve with respect to both the MC simulation and the ordinary P1 approximation; although the latter curves share in common a positive second derivative (a slowing down decay rate) at all depths, the former has a negative second derivative near the boundary. In other words, the MDA predicts a different physical behavior, which deserves some discussion.

If Eq. 15 is analyzed, it is found that, from a mathematical point of view, a negative second derivative may be expected for the MDA approximation in some cases. To get a physical sense of the meaning of this behavior, we have to analyze the situation in more detail; the contributions of beam and diffuse solar radiation are analyzed separately in Figures 5 and 6 (whereas in Figure 4 it was considered that both components impinge in the top of the reactor with the same irradiance). An explanation to the observed behavior can be drawn from these curves. Note that the result of the P1 approximation is not presented in Figure 5, because for purely diffuse incidence, it gives exactly the same results than the MDA. In fact, the P1 method is not able to distinguish between collimated and diffuse radiation.

The behavior displayed in Figure 5 is a relatively simple one, with monotonously increasing slope; that is, second derivative always positive, which is logical, because MDA reduces to the P1 approximation when incidence is purely diffuse. However, for the case with collimated incidence (Figure 6), a negative second derivative of the LVRPA can be appreciated at small depths, both in the MC and in the MDA.

The physical interpretation may be as follows: in a diffuse case, radiation enters and is attenuated by absorption and backscattering at a single rate given by k_d, which continuously reduces the radiative power with depth. On the other hand, when purely collimated radiation is introduced, two different attenuation rates come into play, one for diffuse (in this case $k_d = 17.41$ m^{-1}) and the other for collimated radiation ($\beta = 33.33$ m^{-1}). In fact, diffuse radiation fluxes are absorbed more rapidly with depth than collimated ones, because light rays in them propagate at many different angles with respect to the y axis; that is, their trajectories are longer on the average. On the other hand, diffuse fluxes are not very severely attenuated by scattering, when the asymmetry parameter is greater than zero (as in the present case), because forward scattering does not reduce a diffuse flux. This complicated balance is accounted for in the P1 and

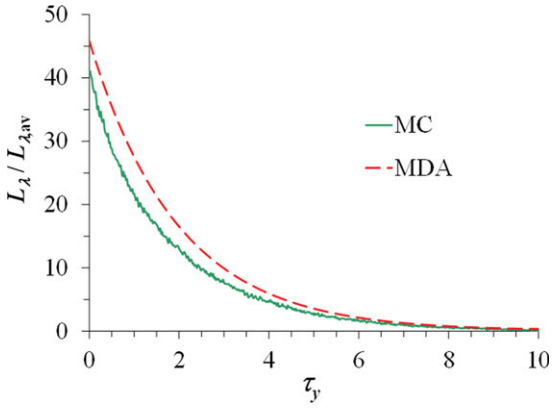

Figure 5. Normalized spectral LVRPA as a function of optical depth coordinate for illumination by purely diffuse solar radiation.

Comparison between different models. [Color figure can be viewed in the online issue, which is available at wileyonlinelibrary.com.]

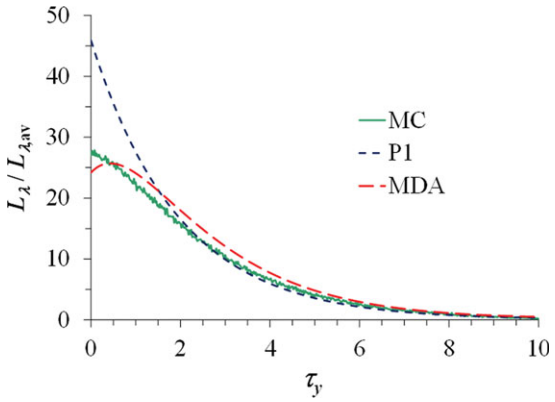

Figure 6. Normalized spectral LVRPA as a function of optical depth coordinate for illumination by purely beam solar radiation.

Comparison between different models. [Color figure can be viewed in the online issue, which is available at wileyonlinelibrary.com.]

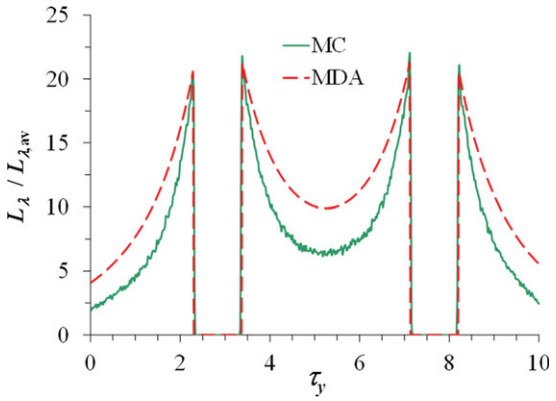

Figure 8. Normalized spectral LVRPA as a function of optical depth coordinate for lamp only illumination.

Comparison between different models. [Color figure can be viewed in the online issue, which is available at wileyonlinelibrary.com.]

MDA approximations by the value of k_d. In the present situation, depicted in Figure 6, diffuse radiation is initially absent, but it starts appearing in the medium, as soon as some of the collimated radiation is scattered by particles and transformed into diffuse.

The above explains the behavior observed for the MC curve in Figure 6: for optical depths smaller than around 0.5, most of the entering radiation is still propagating as a collimated stream of photons. However, for larger optical depths, a significant portion has been transformed by scattering into diffuse radiation, which has a higher attenuation rate. Therefore, the global attenuation rate increases, and the slope becomes more pronounced; that is, a negative second derivative is obtained.

The preceding description corresponds well with the result observed in the MC simulation. However, for the case of the MDA approximation, the change in slope is so pronounced that it leads to a behavior that may seem unphysical at first sight: the increase of the LVRPA with depth (Figure 6). To see that this is not an impossible situation, it is necessary to recall that the LVRPA does not refer to the amount of photons propagating at a given depth but to the amount absorbed per unit volume at each depth. Therefore, if we have a larger average distance traveled by diffuse radiation than by beam radiation, as discussed above, diffuse radiation is also absorbed in larger amounts than collimated one. So, at small optical depths the LVRPA is smaller, because radiation is almost purely beam and is not absorbed very much locally, whereas at larger depths it has transformed mostly into diffuse radiation. Nevertheless, it is clear that the extent of this effect is overestimated by the MDA approximation, as compared to the MC results.

In Figure 7, the effect of the shadowing of solar radiation by the lamps (which are turned off) is presented. The behavior is similar to Figure 4, except for the blocking of radiation by the lamps. Actually, collimated radiation is not allowed to further travel after the first lamp; past the lamp only diffuse radiation exists. The region behind the lamp is thus partially shadowed, and it is refilled progressively by diffuse radiation. This subtle feature is not reproduced by our simplistic application of the MDA results, which evaluates the decay of diffuse radiation as if the lamp was absent. Nevertheless, the approximation is rather accurate in the region

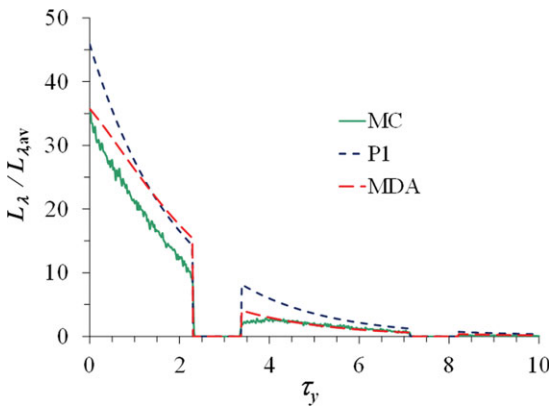

Figure 7. Normalized spectral LVRPA as a function of optical depth coordinate for illumination with global (diffuse plus beam) solar radiation.

Lamps are included but turned off. Comparison between different models. [Color figure can be viewed in the online issue, which is available at wileyonlinelibrary.com.]

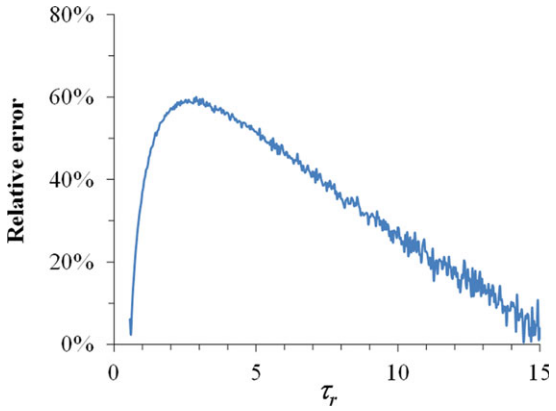

Figure 9. Relative error between MC and MDA predictions for a single isolated lamp in an infinite medium, as a function of radial optical depth from the center of the lamp.

[Color figure can be viewed in the online issue, which is available at wileyonlinelibrary.com.]

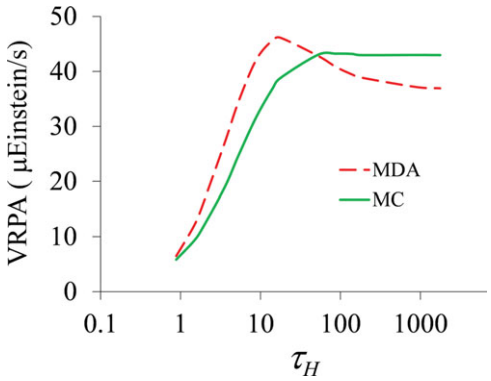

Figure 10. VRPA for lamp only illumination, as a function of optical thickness of the reactor.

MDA vs. MC results. [Color figure can be viewed in the online issue, which is available at wileyonlinelibrary.com.]

between the two lamps, as can be seen in the figure. On the other hand, the simple P1 approximation underestimates the shadowing to the right of the first lamp, because it considers all radiation (including beam) as a diffuse flux.

In Figures 3 and 8, the lamps are turned on. In the first case, only radiation from the lamps is taken into account, with no solar incidence, whereas in the second one, both sources of radiation are considered. For lamp illumination, the disagreement between both methodologies seems to be more important than for solar radiation. As Figure 8 shows, the main differences appear at the midpoint between two lamps. In Figure 9, this situation is examined more closely for the case of a single lamp in a very large reaction space. The relative error between the P1 and MC calculations is depicted. We can see that the greatest difference occurs around at an optical depth value of 2.6 from the lamps, equivalent to a distance of 0.05 cm.

Finally, in Figure 10, as an illustrative example, the VRPA is shown as a function of the vertical optical thickness. The VRPA is the integral of the LVRPA over the whole reactor volume[32]; that is, it gives the number of photons absorbed in the whole reactor per unit time. The case considered is for lamp only illumination, where both MDA and P1 are identical, as discussed above. As can be observed, very significant differences exist between the MDA and the MC results. Both models predict an initial increase of the VRPA with catalyst concentration and a subsequent saturation. This is to be expected: at very low catalyst concentration, the VRPA is small, because photon mean free path is large, and most of the photons escape from the reactor before being absorbed. As concentration increases, the mean free path decreases, eventually eliminating the probability of photon escape. However, aside from this very general behavior, the shape of both curves is very different, as the MDA predicts a high peak that is barely observed in the MC results. Moreover, the saturation values for large concentrations are different in both curves.

As has been discussed previously by Orozco et al.,[7] the reason for the observed maximum is the backscattering toward the lamps produced by the suspended particles: if catalyst concentration is increased too much, the photon mean free path becomes very short. In these conditions, practically all backscattered photons collide with the lamp that emitted them in the first place. These photons are lost, reducing the quantity available for absorption in the volume of the reactor. So, although very few photons are able to escape the reactor, absorption does not saturate at 100%. The observed peak is the result of the complicated tradeoff between the reduction of photons lost to the outside and the increase of those lost to the lamps with increasing concentration. This kind of behavior manifests also for purely solar photoreactors that use cylindrical reaction spaces,[32] where radiation backscattered close to the glass walls has a high probability of escaping the system.

The appearance and extent of the above-described effect is dependent on the distribution of radiation between different propagation directions inside the medium, close to the lamps. This directional distribution is highly oversimplified in the MDA and P1 approximations, and thus it is not strange that they predict results so different from the MC method.

Conclusions

In this report, the absorption of radiation in a HPR operating with solar radiation and lamps has been modeled. Three different methods have been compared: the exact MC solution simulations, the P1 approximation, and the MDA. The latter was used, because the solar radiation impinging in the reactor has an important directional component (beam solar radiation), which is not adequately described by the P1 approximation. In particular, the LVRPA has been evaluated, which is the more relevant radiative quantity in the case of photoreactors. This has been done by taking into account the real absorption and scattering properties of the anatase phase titanium dioxide catalyst, reported in the literature.

As has been stated in the literature,[10] it is found that the P1 approximation fails to describe volumetric absorption near the radiation entrance in the case when important collimated components exist, as in the present case. Moreover, the accuracy of the P1 approximation is seen to improve for larger optical depths inside the reactor, as has also been observed for this kind of approximation.

Surprisingly, when the MDA approximation is applied to correct for the above limitation of the P1 method, the result is not an overall improvement; although the accuracy at the boundary is greatly improved, it is much worsened at medium optical depths. An explanation for this fact has been proposed, in terms of the assumptions of the MDA approximation; these large differences seem to arise from an overestimation of the transformation of collimated radiation into diffuse. In the situation considered here, scattering occurs mainly in the forward direction, which implies that several scattering events are necessary to fully transform a collimated beam into a diffuse one. This is grossly simplified by the MDA approximation, which assumes an immediate transformation of each scattered ray.

According to the above, for the solar component of radiation (rectangular geometry), the MDA approximation provides a better description and more accurate values at very small optical depths, due to its ability to distinguish between beam and diffuse radiation, but at medium optical depths, where most radiation is diffuse, the P1 approximation is a better option. At large optical depths, both approximations have similar accuracy.

With regard to radiation emitted by the lamps, which is purely diffuse, the behavior of the P1 approximation is the opposite: the description is much better near the boundary, worsening at medium optical depths. This latter behavior is harder to explain and probably comes also from the predominance of forward scattering.

Finally, the volumetric rate of energy absorption, integrated over wavelength and reaction volume, has been evaluated for the case of lamp illumination. In this case, there is no difference between the MDA and the P1 methods, but their predictions are very different from the MC results, even at high catalyst concentrations (high optical thicknesses).

Although the above results seem to contradict previous reports,[22] it should be borne in mind that previous comparisons of the P1 and MDA approximations with exact methods like MC have been of a different kind. They have dealt mainly with the evaluation of thermal radiative fluxes exchanged by opaque walls through participating media. In this case, it is the local volumetric absorption of radiation inside the medium that is of interest. We have not found previous reports of such comparisons.

Of course, more comparisons, over a wider range of values of the parameters of the medium, are necessary to assess the general validity of the P1 and MDA to evaluate volumetric absorption distributions. In particular, it has been observed that the optical properties of the catalyst can be significantly affected by the reactor operation conditions.[11,16] Moreover, the determination of the asymmetry parameter, whose value is very important for the present models, may be somewhat ambiguous.[11,12] Nevertheless, it is clear that significant inaccuracies may be incurred by the approximations discussed here.[30] This should be considered as an argument against the indiscriminate use of analytical approximations for the solution of radiative transfer problems. In this sense, as faster personal computers become widely available nowadays, the utilization of exact numerical methods like MC should be strongly advised.

Acknowledgments

S. L. Orozco and H. I. Villafán-Vidales acknowledge CONACYT scholarships. This work was partially supported by CONACYT grants 56918 and 49895-Y. C. A. Arancibia-Bulnes acknowledges support from Universidad de Sonora.

Notation

A = amplitude of the beam component in the solution for solar radiation
B_1 = constant in the solution for solar radiation
B_2 = constant in the solution for solar radiation
c = speed of light in a vacuum
C_{cat} = catalyst concentration, g cm^{-3}
C_1 = constant in the solution for lamps
C_2 = constant in the solution for lamps
C_3 = constant in the solution for lamps
C_4 = constant in the solution for lamps
d = random distance traveled by a photon
D = constant in the solution for solar radiation
e_L = local volumetric rate of photon absorption, E s^{-1} cm^{-3}
E = constant in the solution for solar radiation
g = asymmetry parameter
G, G_λ = local incident radiation, W cm^{-2}
G_c = collimated component of the local incident radiation, W cm^{-2}
G_d = diffuse component of the local incident radiation, W m^{-2}
h = Planck's constant
H = total depth of the reactor, cm
I_c = irradiance of collimated radiation, W cm^{-2}
I_0 = zeroth-order modified Bessel function of the first kind
K_0 = zeroth-order modified Bessel functions of the second kind
K_1 = first-order modified Bessel function of the second kind
k_d = radiation diffusion coefficient, cm^{-1}
L,L_λ = local spectral volumetric rate of photon absorption, E s^{-1} cm^{-3} nm^{-1}
$\hat{\mathbf{n}}$ = unit vector normal to the water–air interface
N_A = Avogadro's number
$N_{i,l}$ = number of lamp photons absorbed at the ith volume element
$N_{i,s}$ = numbers of solar photons absorbed at the ith volume element
N_l = number of emitted lamp photons
N_s = number emitted of solar photons
p_c = fraction of collimated radiation
P_l = power carried by a lamp photon (W)
P_s = power carried by a solar photon (W)
q_c = irradiance of collimated beam at a given depth (W cm^2)
$q_{c,0}$ = impinging irradiance of collimated solar radiation (W cm^2)
$q_{d,0}$ = impinging irradiance of diffuse solar radiation (W cm^2)
Q_l = lamp power input (W)
Q_s = solar power input (W)
r = radial variable for cylindrical coordinates (cm)
$\mathbf{r}$ = position vector (cm)
$\mathbf{r}_i$ = lamp center coordinates (cm)
R = lamp envelope radius (cm)
R_1 = constant in the solution for solar radiation
R_2 = constant in the solution for solar radiation
R_3 = constant in the solution for solar radiation
R_4 = constant in the solution for solar radiation
$\hat{\mathbf{s}}$ = propagation direction unit vector
$\hat{\mathbf{s}}_c$ = collimated radiation propagation direction unit vector
$\hat{\mathbf{t}}_1$ = unit vector perpendicular to the surface normal
$\hat{\mathbf{t}}_2$ = unit vector perpendicular to the surface normal
V_i = volume of the ith volume element (cm^3)
X = width of the reactor (cm)
x = Cartesian coordinate (cm)
Y = height of the reactor (cm)
y = Cartesian coordinate (cm)
Z = length of the reactor (cm)
z = Cartesian coordinate (cm)

Greek letters

β,β_λ = extinction coefficient (cm^{-1})
Γ = nonhomogeneous term of the boundary condition
δ = Dirac's delta function
θ = azimuthal scattering or reflection angle, dummy integration angle (rad)
θ_c = collimated beam azimuthal propagation angle (rad)
κ,κ_λ = absorption coefficient (cm^{-1})
λ = wavelength (nm)
ρ = interface reflectance function
ρ_1 = first moment of the interface reflectance function
ρ_2 = second moment of the interface reflectance function
ρ_c = interface reflectance for collimated radiation
σ,σ_λ = scattering coefficient (cm^{-1})
τ_H = vertical optical thickness of the reaction space
τ_r = radial optical depth
τ_c = optical depth traversed by the collimated beam up to a certain vertical depth
τ_y = optical depth in vertical direction
τ_1 = first moment of the interface transmittance function
τ = transmittance function of the air–water interface
ϕ = cylindrical angular coordinate for lamps (rad)
Φ_λ = phase function
Φ_{HG} = Henyey–Greenstein (HG) phase function
ψ = azimuth angle of reflected or scattered photons (rad)
ω = scattering albedo
Ω = solid angle (srad)

Other symbols

$\Re_i$ = Evenly distributed random number between 0 and 1, for variable i

Literature Cited

1. Herrmann JM. Heterogeneous photocatalysis: fundamentals and applications to the removal of various types of aqueous pollutants. *Catal Today*. 1999;53:115–129.
2. Alfano OM, Bahnemann D, Cassano AE, Dillert R, Goslich R. Photocatalysis in water environments using artificial and solar light. *Catal Today*. 2000;58:199–230.
3. Blanco-Galvez J, Fernández-Ibáñez P, Malato-Rodríguez S. Solar photocatalytic detoxification and disinfection of water: recent overview. *J Solar Energy Eng*. 2007;129:4–15.

4. Bahnemann DW. Photocatalytic water treatment: solar energy applications. *Solar Energy*. 2004;77:445–459.
5. Arancibia-Bulnes CA, Jiménez AE, Estrada CA. *Development and modeling of solar photocatalytic reactors*. In: de Lasa H, Serrano B, editors. *Advances in Chemical Engineering*: Vol. 36, *Photocatalytic Technologies*. Amsterdam: Academic Press, 2009:185–228.
6. Colina-Márquez J, Machuca-Martínez F, Li Puma G. Photocatalytic mineralization of commercial herbicides in a pilot-scale solar CPC reactor: photoreactor modeling and reaction kinetics constants independent of radiation field. *Environ Sci Technol*. 2009;43:8953–8960.
7. Orozco SL, Arancibia-Bulnes CA, Suárez-Parra R. Radiation absorption and degradation of an azo dye in a hybrid photocatalytic reactor. *Chem Eng Sci*. 2009;64:2173–2185.
8. Satuf ML, Brandi RJ, Cassano AE, Alfano OM. Photocatalytic degradation of 4-chlorophenol: a kinetic study. *Appl Catal B: Environ*. 2008;82:37–49.
9. Cabrera MI, Alfano OM, Cassano AE. Absorption and scattering coefficients of titanium dioxide particulate suspensions in water. *Chem Eng J*. 1996;100:20043–20050.
10. Modest MF. *Radiative Heat Transfer*, 2nd ed. San Diego: Academic Press, 2003.
11. Ishimaru A. *Wave Propagation and Scattering in Random Media*. Oxford: Oxford University Press, 1997.
12. Mahan JR. *Radiation Heat Transfer, A Statistical Approach*. New York: Wiley, 2002.
13. Pareek VK, Adesina AA. Light intensity distribution in a photocatalytic reactor using finite volume. *AIChE J*. 2004;50:1273–1288.
14. Romero RL, Alfano OM, Cassano AE. Photocatalytic reactor employing titanium dioxide: from a theoretical model to realistic experimental results. *Ind Eng Chem Res*. 2009;48:10456–10466.
15. Moreira J, Serrano B, Ortiz A, de Lasa H. Evaluation of photon absorption in an aqueous TiO_2 slurry reactor using Monte Carlo simulations and macroscopic balance. *Ind Eng Chem Res*. 2010: 49:10524–10534.
16. Li Puma G, Brucato A. Dimensionless analysis of slurry photocatalytic reactors using two-flux and six-flux radiation absorption-scattering models. *Catal Today*. 2007;122:78–90.
17. Loddo V, Addamo M, Augugliaro V, Palmisano L, Schiavello M, Garrone E. Optical properties and quantum yield determination in photocatalytic suspensions. *AIChE J*. 2006;52:2565–2574.
18. Salaices M, Serrano B, de Lasa HI. Experimental evaluation of photon absorption in an aqueous TiO_2 slurry reactor. *Chem Eng J*. 2002;90:219–229.
19. Yurdakal S, Loddo V, Ferrer BB, Palmisano G, Augugliaro V, Farreras JG, Palmisano L. Optical properties of TiO_2 suspensions: influence of pH and powder concentration on mean particle size. *Ind Eng Chem Res*. 2007;46:7620–76266.
20. Brucato A, Cassano AE, Grisafi F, Montante G, Rizzuti L, Vella G. Estimating radiant fields in flat heterogeneous photoreactors by the six-flux model. *AIChE J*. 2006;52:3882–3890.
21. Arancibia-Bulnes CA, Bandala ER, Estrada CA. Radiation absorption and rate constants for carbaryl photocatalytic degradation in a solar collector. *Catal Today*. 2002;76:149–159.
22. Arancibia-Bulnes CA, Cuevas SA. Modeling of the radiation field in a parabolic trough solar photocatalytic reactor. *Solar Energy*. 2004;76:615–622.
23. Villafán-Vidales HI, Cuevas SA, Arancibia-Bulnes CA. Modeling the solar photocatalytic degradation of dyes. *J Solar Energy Eng Trans ASME*. 2007;129:87–93.
24. Cuevas SA, Arancibia-Bulnes CA, Serrano B. Radiation field in an annular photocatalytic reactor by the P1 approximation. *Int J Chem Reactor Eng*. 2007;5:5801–5814.
25. Ravishankar M, Mazumder S, Sankar M. Application of the modified differential approximation for radiative transfer to arbitrary geometry. *J Quant Spectrosc Radiat Transfer*. 2010;111:2052–2069.
26. Modest MF. The modified differential approximation for radiative transfer in general three-dimensional media. *J Thermophys Heat Transfer*. 1989;3:283–288.
27. Satuf ML, Brandi RJ, Cassano AE, Alfano OM. Experimental method to evaluate the optical properties of aqueous titanium dioxide suspensions. *Ind Eng Chem Res*. 2005;44:6643–6649.
28. Hulstrom R, Bird R, Riordan C. Spectral solar irradiance data sets for selected terrestrial conditions. *Solar Cells*. 1985;15:365–391.
29. Marshak RE. Note on the spherical harmonic method as applied to the Milne problem on a sphere. *Phys Rev*. 1947;71:443–446.
30. Spott T, Svaasand LO. Collimated light sources in the diffusion approximation. *Appl Opt*. 2000;39:6453–6465.
31. Li Puma G, Puddu V, Tsang HK, Gora A, Toepfer B. Photocatalytic oxidation of multicomponent mixtures of estrogens (estrone (E1), 17β-estradiol (E2), 17α-ethynylestradiol (EE2) and estriol (E3)) under UVA and UVC radiation: photon absorption, quantum yields and rate constants independent of photon absorption. *Appl Catal B: Environ*. 2010;99:388–397.
32. Colina-Márquez J, Machuca-Martínez F, Li Puma G. Radiation absorption and optimization of solar photocatalytic reactors for environmental applications. *Environ Sci Technol*. 2010;44:5112–5120.

Appendix

By substituting the general solutions to the MDA equation into the boundary condition (10), the various constants are obtained. For instance, the coefficients for the solution of Eq. 15 are given by

$$C_1 = \frac{(D - E - AR_3)R_1 \exp(k_d H) + AR_2R_4 \exp(-\beta H/\cos\theta_c)}{R_1^2 \exp(k_d H) - R_2^2 \exp(-k_d H)} \tag{A1}$$

and

$$C_2 = -\frac{(D - E - AR_3)R_2 \exp(-k_d H) + AR_1R_4 \exp(-\beta H/\cos\theta_c)}{R_1^2 \exp(k_d H) - R_2^2 \exp(-k_d H)} \tag{A2}$$

where H is the reactor height, and several other constants have been defined

$$R_1 = (1 - 2\rho_1) + 2k_d(1 + 3\rho_2)[3\beta(1 - \omega g)]^{-1} \tag{A3}$$

$$R_2 = (1 - 2\rho_1) - 2k_d(1 + 3\rho_2)[3\beta(1 - \omega g)]^{-1} \tag{A4}$$

$$R_3 = (1 - 2\rho_1) + 2(1 + 3\rho_2)[3\cos\theta_c(1 - \omega g)]^{-1} \tag{A5}$$

$$R_4 = (1 - 2\rho_1) - 2(1 + 3\rho_2)[3\cos\theta_c(1 - \omega g)]^{-1} \tag{A6}$$

$$D = 8\tau_1 q_{d,o} \tag{A7}$$

$$E = 2\omega g(1 + 3\rho_2)(1 - \rho_c)q_{c,0} \cos\theta_c(1 - \omega g)^{-1} \tag{A8}$$

In particular, when there is no collimated incidence, $A = E = 0$ and the coefficients of the solution (18) are obtained

$$B_1 = \frac{DR_1}{R_1^2 - R_2^2 \exp(-2k_d H)} \tag{A9}$$

$$B_2 = -\frac{DR_2}{R_1^2 \exp(2k_d H) - R_2^2} \tag{A10}$$

Finally, for the solution of the lamps contribution (21), the coefficient is given by

$$C_4 = 4q_{d,0}\left[(1 - 2\rho_1)K_0(k_d R) + \frac{2k_d(1 + 3\rho_2)}{3\beta(1 - \omega g)}K_1(k_d R)\right]^{-1} \tag{A11}$$

Manuscript received Apr. 1, 2011, and revision received Nov. 21, 2011.